Available online at www.sciencedirect.com

ScienceDirect

Nuclear Physics A 979 (2018) 102–112

NUCLEAR PHYSICS A

www.elsevier.com/locate/nuclphysa

Excitation function of the $p + {}^{nat}Ag$ reactions in the energy range 10–22 MeV

Siddharth Parashari [a,*], S. Mukherjee [a], S.V. Suryanarayana [b], R. Makwana [a], B.K. Nayak [b], A. Shanbhag [b], H. Naik [c]

[a] *Department of Physics, Faculty of Science, The M. S. University of Baroda, Vadodara - 390002, India*
[b] *Nuclear Physics Division, Bhabha Atomic Research Center, Mumbai - 400085, India*
[c] *Radiochemistry Division, Bhabha Atomic Research Center, Mumbai - 400085, India*

Received 27 July 2018; received in revised form 12 September 2018; accepted 13 September 2018
Available online 20 September 2018

Abstract

The excitation functions of the proton induced ^{nat}Ag reactions were measured using the stack foil activation followed by the off-line γ-ray spectrometry. The present work was carried out at 14UD BARC-TIFR Pelletron accelerator, Mumbai, India. The proton beam of 22 MeV was used for the irradiation of the samples and was degraded along the stack of silver foils. The measured cross-section data were compared with the existing literature data available in EXFOR. The calculated excitation functions were also compared with the calculated values from TALYS-1.9 model code using a suitable input parameters for the pure compound nucleus (CN) and pre-equilibrium (PE) reaction cross-sections. ALICE-2014 code was also used to validate the present experimental findings as well as the TALYS-1.9 results.

Keywords: $^{nat}Ag(p, x)$ reactions; Stack foil activation; Off-line γ-ray spectrometry; TALYS-1.9; ALICE-2014; Pre-equilibrium emission

* Corresponding author.
E-mail addresses: siddharthparashri5@gmail.com (S. Parashari), sk.mukherjee-phy@msubaroda.ac.in (S. Mukherjee).

https://doi.org/10.1016/j.nuclphysa.2018.09.042
0375-9474/

1. Introduction

Silver is a soft, white, lustrous transition metal. It also exhibits the highest electrical conductivity, thermal conductivity, and reflectivity of any metal. Silver is also an essential component of the different alloys which are commonly used in nuclear technology. This metal can be found in the earth's crust in the pure, free elemental form (native silver), as an alloy with other metals like gold, and in mineral form with its two stable isotopes ^{107}Ag (51.839%) and ^{109}Ag (48.161%) [1]. Most of the silver is produced as a byproduct of copper, gold, lead, and zinc refining. The excitation functions of the proton-induced reactions on silver isotopes are of keen interest in various scientific applications, like accelerator technology, charged particle activation analysis, medical applications, thin layer activation analysis (TLA) [2–4] and to test theoretical nuclear models. The long-lived activities produced in the silver target are also crucial for the management of radiotoxic waste for modern nuclear technology.

Silver isotopes are widely used for the production of some very important medical radionuclides like ^{103}Pd and ^{101}Rh [5,6]. These isotopes are extensively used in the prostate cancer, intra-vascular brachytherapy and the other types of tumors [7]. The ^{101m}Rh nuclide has some applications as the anti-tumor and a chemotherapeutic agent. The proton induced reactions with silver targets provide some important alternative routes for the production of different radioisotopes of Cd, Pd, and Rh, which are important for the advancement of the medical accelerators and the fast reactors. The chemical and metallic properties of silver make it a suitable candidate to be used in the advanced fast nuclear reactor technology. One of the significant application to study the single charged particle induced reactions with silver targets is to test and provide some useful outcomes for the theoretical model codes. This also serves an excellent opportunity to perform a comparative study among the different nuclear model codes, experimental data and the data from different data libraries. Very few experimental investigations are available for the $p + Ag$ reactions at low and medium energies [2,8]. However, several experimental findings are available in the literature for high energy proton-induced reactions of Ag [3,4,8]. The accurate measurement of the proton flux forms an important parameter. In spite of these, the cross-section data with natural silver targets are very much limited. Earlier a few authors [2,8] have used the monitor reaction for the measurement of the proton flux. Therefore, the measured data is strongly correlated with the monitor reaction cross-sections, and hence, larger uncertainties may possibly reflect in the results [9]. To avoid the large uncertainties and the correlations among the measured data, we have calculated the proton flux using the charge collected on the Faraday cup and by monitoring the proton beam current during the course of the experiment.

In the present work, we have studied the excitation functions of proton induced reactions on natural silver target within the projectile energy range of 10–22 MeV. The motivation for the present study was to measure the cross-section of produced radioisotopes at the available excitation energies. Besides this, a comparison of the present reactions with the theoretical value based on TALYS-1.9 [10] and ALICE-2014 [11,12] codes has been carried out. It was observed from our previous work [13] that there may be a significant PE contribution in the formation of the radioisotopes at the energies under consideration. Therefore, in the present measurement, we have also examined the probable pre-equilibrium effects at 10–22 MeV projectile energies. Different level density models available in TALYS-1.9 [10] and ALICE-2014 [11,12] were also tested for the reproduction of the experimental data.

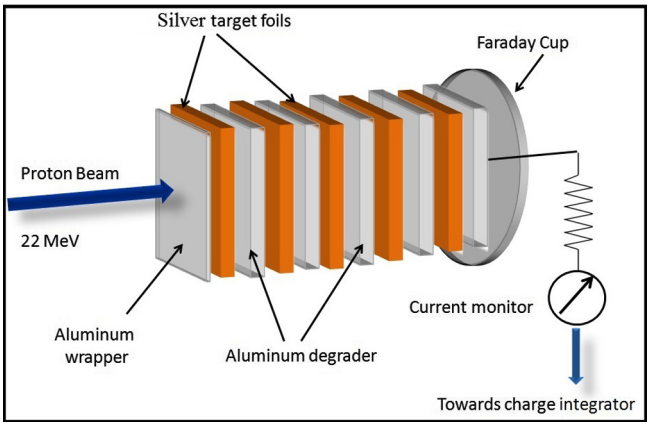

Fig. 1. (Color online.) The schematic diagram of the experimental setup of stacked foil activation technique.

2. Experimental methodology

The measurement of the excitation functions for the present experiment was carried out by using the stack foil activation technique [14,15] followed by off-line γ-ray spectroscopy at 14UD Bhabha Atomic Research Center-Tata Institute of Fundamental Research (BARC-TIFR) Pelletron facility in Mumbai, India. High purity ($\approx 99.98\%$) natural silver foils of thickness ≈ 32 μm were used as target. Aluminum foils of appropriate thickness were applied after each Ag target foil to reduce the beam energy significantly. The proton energy degradation on different targets along the stack was calculated by SRIM code [16]. A schematic diagram of the stack is presented in Fig. 1. The stack wrapped in thin aluminum foil was kept inside the 6 m irradiation port, just before the analyzing magnets on the main beam line of the Pelletron. This port is most suitable for the irradiation experiments, which require high proton flux. The proton beam was made to pass through a thick Ta collimator of 6 mm diameter to get a proper circular shaped beam. The stack was irradiated for 2–2.5 h with a constant proton current of 180 nA to build up sufficient activity. The proton flux during the irradiation was calculated from the charge collected on a Faraday cup and using current as well. In order to reduce the radioactive dose before recording the γ-ray spectra, the irradiated samples were allowed to cool for few hours. Each sample was counted for about 1 h by using a pre-calibrated 80 cm^3 HPGe detector coupled to a PC based 4096 channel analyzer. The counting of targets for a longer time helps reducing the uncertainty in counting statistics. The irradiated samples were placed at a distance of 5 cm from the detector end cap to avoid the summing effect and to reduce the dead time of the detector. The HPGe detector was calibrated with a standard ^{152}Eu source. The resolution of the detector system during counting was measured as 1.82 keV at 1332 keV of ^{60}Co. The counting of the samples was repeated over a period of time according to the decay half-life of the reaction products. The characteristic γ-lines with their respective half-lives were used to identify the residual nuclei of interest. All the spectroscopic data used in the present calculations were taken from NuDat [17] database, whereas the Q-values and the threshold energies were taken from Qtool [18], which are summarized in Table 1.

Table 1
List of identified residues in the $p + {}^{nat}Ag$ reactions with their spectroscopic data [17] and reaction threshold energy [18].

Nuclide	$T_{1/2}$	Decay mode (%)	E_γ (keV)	I_γ (%)	Channel	E_{th} (MeV)
${}^{107}Cd$	6.50 ± 0.02 h	$\varepsilon(100\%)$	93.12 ± 0.02	4.8 ± 0.3	${}^{107}Ag(p,n)$	2.21
					${}^{109}Ag(p,3n)$	18.82
${}^{106g}Ag$	23.96 ± 0.04 min	$\varepsilon(99.5\%)$	–	–	–	–
		$\beta^-(<1\%)$	–	–	–	–
${}^{106m}Ag$	8.28 ± 0.02 days	$\varepsilon(100\%)$	450.98 ± 0.02	28.2 ± 0.7	${}^{107}Ag(p,d)$	7.37
			616.17 ± 0.03	21.6 ± 0.6	${}^{107}Ag(p,pn)$	9.62
			717.24 ± 0.09	28.9 ± 0.8		
			748.44 ± 0.11	20.6 ± 0.6		

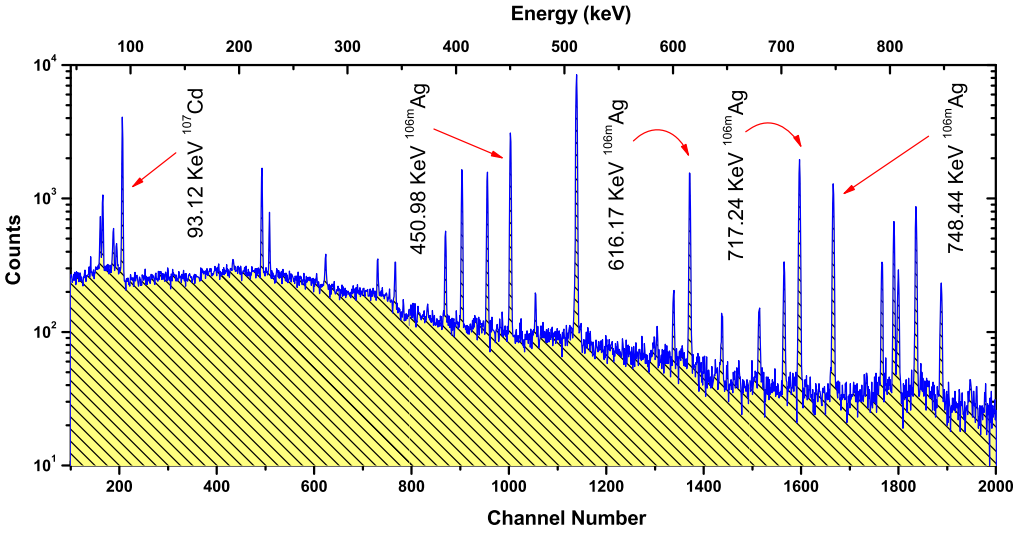

Fig. 2. (Color online.) A typical γ-ray energy spectrum obtained from the interaction of $p + {}^{nat}Ag$ at $E_{Lab} \approx 17$ MeV.

3. Data analysis

The excitation functions in the proton induced reaction of ${}^{nat}Ag$ were measured at five energies within the range 10–22 MeV. The mid-point energy for each Ag foil was calculated by SRIM code [16] and were found to be 21.82 ± 0.17, 19.48 ± 0.18, 16.77 ± 0.20, 13.90 ± 0.23, and 11.13 ± 0.28 MeV, respectively. In the present study, we have identified two reaction residues, ${}^{107}Cd$ and ${}^{106m}Ag$. The radionuclide ${}^{107}Cd$ was found to be populated through ${}^{107}Ag(p,n)$ and ${}^{109}Ag(p,3n)$ reaction channels with the thresholds of 2.21 and 18.82 MeV, respectively. On the other hand, the residue ${}^{106m}Ag$, which is populated through the ${}^{107}Ag(p,d)$ and ${}^{107}Ag(p,pn)$ reaction channels with the thresholds of 7.37 and 9.62 MeV, respectively. All these residues were identified through their characteristic γ-lines [17] and by following their half-lives [17]. A typical recorded γ-ray spectrum for the ${}^{nat}Ag$ sample irradiated at $\approx$17 MeV proton energy is shown in Fig. 2. The radionuclide ${}^{107}Cd$ has a half-life of 6.50 ± 0.02 h. The γ-line of

93.12 ± 0.02 keV (4.8 ± 0.3%) was used to evaluate the cross-sections for the $^{nat}Ag(p,x)^{107}Cd$ reaction. However, ^{106}Ag has the ground state as well as the metastable state. The ground state of ^{106}Ag has a half-life of 23.96 ± 0.04 min, which is very short as compared to its metastable state (8.28 ± 0.02 days). The transition of ^{106m}Ag is due to the β^+(100%) decay into the ^{106}Pd daughter nucleus. The longer half-life of the ^{106m}Ag enabled us to perform the repeated counting of the Ag targets before it decays to the ground state. The four γ-line energies of 450.98 ± 0.02 (28.2 ± 0.7%), 616.17 ± 0.03 (21.6 ± 0.6%), 717.24 ± 0.09 (28.9 ± 0.8%) and 748.44 ± 0.11 (20.6 ± 0.6%) keV, respectively, were used for the measurement of the cross-sections for the $^{nat}Ag(p,x)^{106m}Ag$ reaction. The final cross-section for the $^{nat}Ag(p,x)^{106m}Ag$ reaction was opted by taking the weighted average of the cross-sections from each of the four gamma lines under consideration. All the details related to spectroscopic data are presented in Table 1. The photo-peak counts from each γ-lines described above were used to calculate the reaction cross-sections for each residue by using the following expression,

$$\sigma_R = \frac{C_{obs}(C_L/L_T)\lambda}{N_0\epsilon I_\gamma \phi K(1-e^{-\lambda T_i})(e^{-\lambda T_c})(1-e^{-\lambda T_{LT}})} \tag{1}$$

where, σ_R is the reaction cross-section, C_{obs} is the photo peak counts of the gamma line of interest, C_L, L_T are the clock time and the live time for the counting of the spectrum, λ is the decay constant, I_γ is the branching ratio for the each γ-ray taken from Ref. [17], N_0 is the total number of target nuclei in the sample, ϵ is the detector efficiency and ϕ is the proton flux. $K = [1-exp(-\mu d)]/(\mu d)$ is the correction factor for the self-absorption of γ-rays in the sample thickness 'd' with the absorption coefficient μ.

4. Theoretical framework

4.1. Theoretical calculations by using the TALYS-1.9 code

The cross-section for the $^{nat}Ag(p,x)^{107}Cd$ and the $^{nat}Ag(p,x)^{106m}Ag$ reactions as a function of proton energy from their respective thresholds to 50 MeV were calculated by using the TALYS-1.9 code [10]. This code is the most useful theoretical nuclear model code, which is being used worldwide for nuclear reaction cross-section data prediction. It can successfully reproduce the nuclear reaction cross-section, and the other data for the light particles induced reactions on incident particle energies up to 200 MeV. TALYS code takes the reaction parameters from the Reference Input Parameter Library (RIPL) database [19]. The code accounts for various reaction mechanisms like; compound nucleus, pre-equilibrium, and direct reactions. It also accounts for the effects of level density as a function of incident particle energy. TALYS-1.9 is equipped with the optical model parameters by using a global potential, which was proposed by Koning and Delaroche [20]. The Hauser–Feshbach model [21] takes care of the compound nuclear reaction using the exciton model, which was developed by Kalbach [22] and is used to accommodate the pre-equilibrium contribution.

4.2. Theoretical calculations by using the ALICE-2014 code

The cross-sections for the $^{nat}Ag(p,x)^{107}Cd$ and the $^{nat}Ag(p,x)^{106m}Ag$ reactions as a function of proton energy from their respective thresholds to 50 MeV were theoretically calculated by using the ALICE-2014 [11,12] code. This code is based on the Hybrid Monte-Carlo Simulation (HMS) pre-compound decay [23], Weisskopf–Ewing evaporation [24], Bohr–Wheeler

Table 2
Experimentally measured cross-sections for the identified reaction residues.

Proton energy (MeV)	$^{106}Ag(p,x)^{107}Cd$ (mb)	$^{106}Ag(p,x)^{106m}Ag$ (mb)
11.13 ± 0.28	222.52 ± 20.44	–
13.90 ± 0.23	175.59 ± 16.85	0.218 ± 0.215
16.77 ± 0.20	47.76 ± 4.63	11.21 ± 0.93
19.48 ± 0.18	28.45 ± 2.25	$30.57 \pm 0.2.65$
21.82 ± 0.17	104.18 ± 9.89	52.14 ± 4.74

[25] fission models and the angular distribution was incorporated by the linear momentum conservation model of Chadwick and Oblozinsky [26]. ALICE-2014 is a much-advanced version, and it uses the Monte Carlo simulation technique to reproduce the reaction data. The code accepts incident particles from neutron, proton, and gamma to heavy-ions and it works flawlessly up to 250 MeV incident particle energies. The code uses mainly three level densities such as Fermi gas, backshifted pairing energies, Kataria–Ramamurthy and Obninsk. The level density parameter (PLD) can be changed in order to get the most significant fit for the experimental data.

In the present work, the experimental data were compared by the cross-sections reproduced by activating different level density models (ldmodel 1–3) present in TALYS-1.9 [10]. The different level densities in TALYS (ldmodel 1–3) account for, Constant Temperature Fermi gas model (CTFGM) [27], Back-shifted Fermi gas model (BSFGM) [28], Generalised superfluid model (GSFM) [29,30], respectively. The present data were also compared with the theoretical predictions from ALICE-2014 [11,12] using the obninks level density model. The level density parameter was chosen as 9, which is set as default for each level density model in the ALICE-2014 [11,12] model code. The PE contribution was calculated by using the exciton model [31] (preeqmode3) present in the TALYS-1.9 [10] model code. The ALICE-2014 model code was also used to verify the pre-equilibrium contribution present in the experimental cross-sections and that calculated by the TALYS-1.9 model code.

5. Results and discussion

In the present paper, the excitation function for the proton induced ^{nat}Ag reactions were measured at the five proton energies of 21.82 ± 0.17, 19.48 ± 0.18, 16.77 ± 0.20, 13.90 ± 0.23 and 11.13 ± 0.28 MeV, respectively. The experimentally measured cross-sections for both the residue are summarized in Table 2. The calculated cross-sections were also compared with the literature data available in EXFOR [32] and the theoretical results were obtained by using the TALYS-1.9 [10], and ALICE-2014 [11,12] model codes. The uncertainties in the present measurement were calculated as the quadratic sum of both statistical and systematic uncertainties. The statistical error serves as the primary source of uncertainty in the measurement and was estimated to be $< 5\%$. The statistical error was reduced by performing the counting of each sample for a significant time. There could be various sources of the systematic uncertainty in the measured cross-sections. The dead time of the HPGe detector was kept $< 2\%$ by adjusting the sample to detector distance. An uncertainty may appear due to the solid-angle effect, as the irradiated samples were not point-source like the ^{152}Eu standard source but had a finite diameter, and it is found to be $< 5\%$. The fluctuations in the beam current may result in the uncertainty in

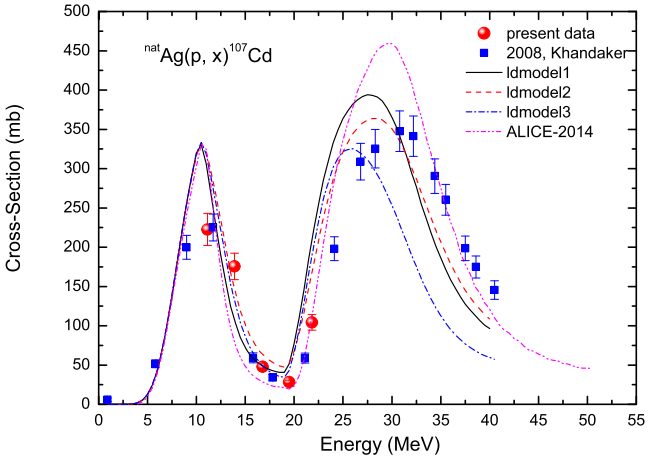

Fig. 3. (Color online.) Excitation function of $^{nat}Ag(p,x)^{107}Cd$ reaction. The comparison of the present and the literature data [8] with different level density model parameters (ldmodel 1–3) in TALYS-1.9 [10] and ALICE-2014 [11,12] default values.

incident flux. The current was kept constant during the irradiation, and the error due to the flux is estimated to be $< 3\%$. The inaccurate estimation of the foil thickness may lead to the uncertainty in determining the number of target nuclei and comes out to be $< 3\%$. The overall error in the present measurements have been estimated to be $< 10\%$.

5.1. Excitation function of the $^{nat}Ag(p,x)^{107}Cd$ reaction

The present experimental results were compared with the literature data [8] and the theoretical reproduction using the model codes TALYS-1.9 [10] and ALICE-2014 [11,12]. Three different level density models (ldmodel 1–3) were used in the TALYS-1.9 calculations. The cross-section data for the $^{nat}Ag(p,x)^{107}Cd$ reaction are plotted in Fig. 3. From Fig. 3, it can be noted that the experimental data were found in fairly good agreement with the literature data [8] from the EXFOR [32] compilation. It can also be seen that only one experimental finding available in the literature for the production cross-sections of ^{107}Cd radioisotope using natural Ag as the target material. The first peak in the Fig. 3 corresponds purely to the (p,n) channel from the ^{106}Ag isotope, however, both the $^{106}Ag(p,n)$ and $^{109}Ag(p,3n)$ channels contribute to the second peak. The dip in the reaction cross-sections around 20 MeV is due to the opening of the $^{109}Ag(p,3n)$ reaction channel around 18 MeV. The nuclear model codes; TALYS-1.9 [10] and ALICE-2014 [11,12] were found to be successful in order to reproduce the reaction cross-section data up to 25 MeV. Beyond 25 MeV energies, the codes were only able to reproduce the trend of the data, however, the broadening of the second peak in the Fig. 3 may be due to the admixture of the $(p,3n)$ channel coming from the ^{109}Ag, and can be fitted by using a more rigorous calculations in TALYS-1.9. Among the different level density model used for the present calculations, the Back-shifted Fermi gas model (ldmodel 2) [28] was found to be successful in order to reproduce the experimental data. The ALICE-2014 [11,12] code also provides the similar trend for the cross-sections except for the second peak in Fig. 3, which corresponds to the $^{109}Ag(p,3n)^{107}Cd$ reaction channel.

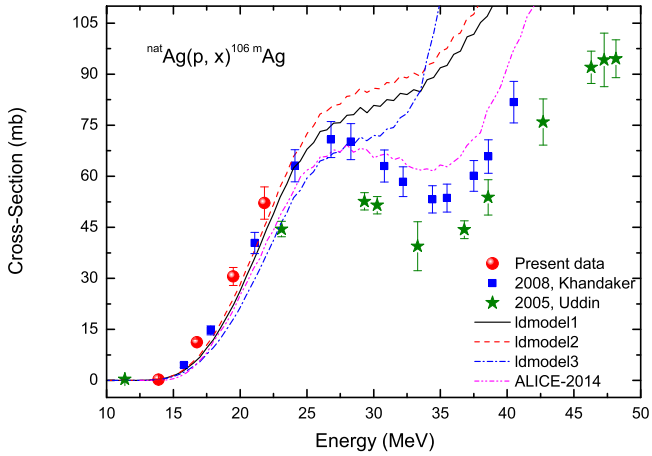

Fig. 4. (Color online.) Excitation function of $^{nat}Ag(p,x)^{106m}Ag$ reaction. The comparison of the present and the literature data [2,8] with different level density model parameters (ldmodel 1–3) in TALYS-1.9 [10] and ALICE-2014 [11,12] default values.

5.2. *Excitation function of the $^{nat}Ag(p,x)^{106m}Ag$ reaction*

The excitation function of the $^{nat}Ag(p,x)^{106m}Ag$ reaction is shown in Fig. 4. It can be observed from the Fig. 4 that the present results are in consensus with the literature data [2,8]. The data from Uddin et al. [2] and from Khandaker et al. [8] were also found in a general agreement. However, the data from Khandaker et al. [8] were found to be enhanced to a small degree. The minor disagreement between both the data [2,8] can arise from the different flux values used from the monitor reaction. The theoretical data from TALYS-1.9 [10] were found significantly higher than the experimental results. On the other hand, the experimental results are very well reproduced by the ALICE-2014 [11,12] model code calculations in the present energy region of 10 to 22 MeV. The different level density models were also tested by using the TALYS-1.9 [10] model code to reproduce the reaction cross-section data successfully up to 30 MeV. Furthermore, the ALICE-2014 [11,12] model code was found more accurate in the theoretical calculations of the reaction cross-section data for an almost entire range of the proton energies under consideration. It may be observed that the TALYS-1.9 code shows an overestimation in the PE contribution and that increases with the increase in the proton energy. To investigate the observed disagreement between the experimental and the theoretical data, the PE calculations have been performed using the pre-equilibrium exciton model [31] (preeqmode3) and the pure compound nucleus reaction cross-sections were calculated by switching off the PE in the TALYS-1.9 code [10].

The PE calculations were performed using the exciton model [31], which takes the numerical transition rates with an optical model for collision probability. The pure compound nucleus (CN) contribution was calculated using TALYS-1.9 [10] by switching off the PE part. The results from the default, modified input in TALYS-1.9 [10] together with the results of ALICE-2014 [11,12] are plotted in Figs. 5 and 6 for production cross-sections of ^{107}Cd and ^{106m}Ag radionuclide, respectively. From Fig. 5, it can be observed that the default, CN, and PE with mode3 all were found in good agreement with the experimental data up to 22 MeV. Beyond 22 MeV, only the default from TALYS-1.9 [10] was found to explain the trend of the measured and literature data. However, in the case of ^{106m}Ag, it can be seen from Fig. 6 that the TALYS with PE mode 3

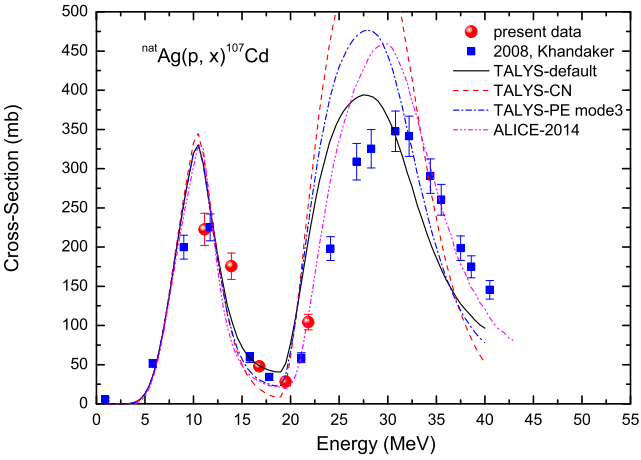

Fig. 5. (Color online.) Excitation function of $^{nat}Ag(p,x)^{107}Cd$ reaction. The comparison of the present and the literature data [2] with pure CN and CN+PE reaction cross-sections from TALYS-1.9 [29] and default values from ALICE-2014 [11,12].

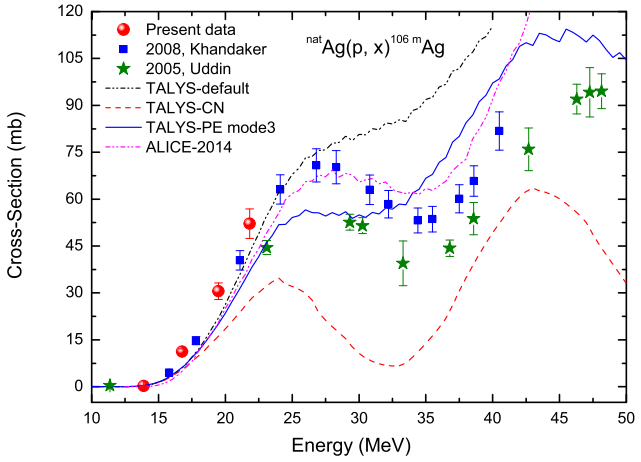

Fig. 6. (Color online.) Excitation function of $^{nat}Ag(p,x)^{106m}Ag$ reaction. The comparison of the present and the literature data [2,8] with pure CN and CN+PE reaction cross-sections from TALYS-1.9 [29] and default values from ALICE-2014 [11,12].

[31] was found to be the closest among all the models of TALYS-1.9 [10] and ALICE-2014 [11, 12] in order to interpret the experimental data. It is also evident from the above discussion that there is a significant contribution from the PE emission in the production of both the residues. Therefore, to investigate this, we have calculated the pre-equilibrium contribution (PE%) present in each case as a function of projectile energy and is plotted in Fig. 7. The PE% can be stated as the ratio of PE cross-section to the evaporation residue cross-section. It can be seen from the Fig. 7 that the PE contribution starts at around 13 MeV and increases with the projectile energy. However, after a small increment, the PE% starts to die out in both the ^{107}Cd and ^{106m}Ag isotopes. The rapid decrease in PE% can be a signature of opening up of $^{109}Ag(p,3n)^{107}Cd$ and

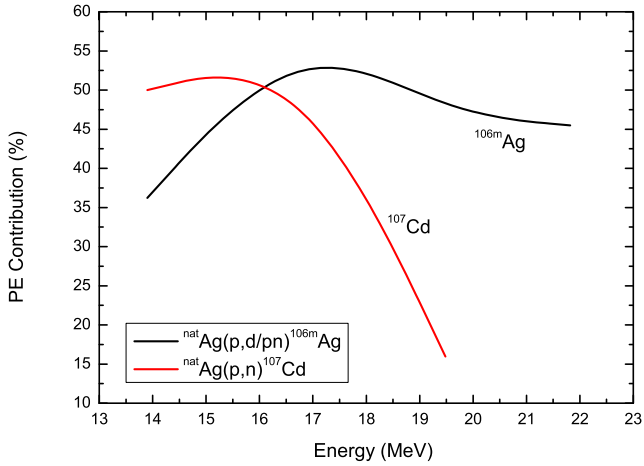

Fig. 7. (Color online.) The estimated PE (%) contribution from the present data as a function of projectile energy.

$^{107}Ag(p, pn)^{106m}Ag$ channels. Furthermore, the PE contribution was found to be greater for the reaction that consists fewer particles in the exit channel and has a small threshold value. It can also be stated that the PE emission directly depends on the initial excitation energy or the Q-value of the reaction.

6. Conclusions

In the present work, the excitation function of the $^{nat}Ag(p, x)$ reactions were determined experimentally using the stack foil activation technique at five proton energies of 21.82 ± 0.17, 19.48 ± 0.18, 16.77 ± 0.20, 13.90 ± 0.23 and 11.13 ± 0.28 MeV, respectively. We have calculated the flux directly from the charge integrator and current using the Faraday cup instead of using any monitor reaction. Different level density models in TALYS-1.9 and the nuclear model code ALICE-2014 have been tested for the reactions of present study. The experimental data were found to be in good agreement with the literature data and the theoretical values calculated using TALYS-1.9 and ALICE-2014 codes. It was observed that ALICE-2014 values were in general more accurate to reproduce the experimental data. On the other hand, TALYS-1.9 can provide a better insight into the PE calculations as it contains different models for the theoretical calculations. It is also needed to be mentioned that, the calculation of PE contribution is vital for the proton/neutron induced reactions at such higher energies. The precise measurement of the nuclear reaction data is the key tool for the future medical accelerators and reactor development. The present work is also essential for the dose estimation and the production cross-section measurement of medical isotopes using ^{nat}Ag target.

Acknowledgements

One of the authors (SM) thanks to the DAE-BRNS for the sanction of a major research project (Sanction Number: 36(6)/14/22/2016-BRNS) as well as providing fellowship to the author (SP). The authors are thankful to Prof. V. Nanal and the staff of the Pelletron facility TIFR, Mumbai for their excellent operation of the accelerator and other supports during the experiment. The au-

thors are also thankful to Dr. G.F. Steyn (iThemba Lab South Africa) for providing ALICE-2014 calculations.

References

[1] Chart of Nuclides, National Nuclear Data Center, Brookhaven National Laboratory, https://www.nndc.bnl.gov/chart/.
[2] M.S. Uddin, M. Hagiwara, M. Baba, F. Tarkanyi, F. Ditroi, Appl. Radiat. Isot. 62 (2005) 533–540.
[3] M.S. Uddin, M. Hagiwara, F. Tarkanyi, F. Ditroi, M. Baba, Appl. Radiat. Isot. 60 (2004) 911–920.
[4] M.S. Uddin, M. Hagiwara, N. Kawata, T. Itoga, N. Hirabayashi, M. Baba, F. Tarkanyi, F. Ditroi, J. Csikai, J. Nucl. Sci. Tech. Suppl. 4 (2004) 160–163.
[5] M. Fassbender, et al., Radiochim. Acta 87 (1999) 87–91.
[6] J.C. Blasko, P.D. Grimm, H. Ragde, Semin. Radiat. Oncol. 3 (4) (October 1993) 240–249.
[7] P. Grimm, J. Sylvester, Rev. Urol. 6 (Supp. 4) (2004) 37.
[8] M.U. Khandaker, K. Kim, K.-S. Kim, M. Lee, G. Kim, Y.S. Cho, Y.O. Lee, Nucl. Instrum. Methods Phys. Res. B 266 (2008) 5101.
[9] S. Parashari, et al., Phys. Rev. C 98 (2018) 014625.
[10] A.J. Koning, S. Hilaire, S. Goriely, TALYS user manual, A nuclear reaction program, NRG-1755 ZG PETTEN, The Netherlands, 2015.
[11] M. Blann, Phys. Rev. Lett. 27 (1971) 337.
[12] M. Blann, Phys. Rev. Lett. 28 (1972) 757.
[13] S. Parashari, et al., Nucl. Phys. A 978 (2018) 160–172.
[14] Harish Kumar, Suhail A. Tali, M. Afzal Ansari, D. Singh, Rahbar Ali, Kamal Kumar, N.P.M. Sathik, S. Parashari, Asif Ali, R. Dubey, Indu Bala, Rakesh Kumar, R.P. Singh, S. Muralithar, Nucl. Phys. A 960 (2017) 53.
[15] S.A. Tali, H. Kumar, M.A. Ansari, A. Ali, D. Singh, R. Ali, Pankaj K. Giri, Sneha B. Linda, S. Parashari, R. Kumar, R.P. Singh, S. Muralithar, Nucl. Phys. A 970 (2018) 208–223.
[16] J.F. Ziegler, SRIM08, The Stopping and Range of Ions in Matter, http://www.srim.org/, 2008.
[17] NuDat 2.7β 2011, National Nuclear Data Center, Brookhaven National Laboratory, https://www.nndc.bnl.gov/nudat2/.
[18] Qtool: calculation of reaction Q-values and threshold, Los Alamos National Library, http://cdfe.sinp.msu.ru/services/calc_thr/calc_thr.html.
[19] R. Capote, et al., Nucl. Data Sheets 110 (2009) 3107.
[20] A.J. Koning, J.P. Declaroche, Nucl. Phys. A 713 (2003) 231.
[21] W. Hauser, H. Feshbach, Phys. Rev. 87 (1952) 366.
[22] C. Kalbach, Phys. Rev. C 33 (1986) 818.
[23] M. Blann, Phys. Rev. C 54 (1996) 1341.
[24] V.F. Weisskopf, D.E. Ewing, Phys. Rev. 57 (1940) 472.
[25] N. Bohr, J.A. Wheeler, Phys. Rev. 56 (1939) 426.
[26] M.B. Chadwick, P. Oblozinsky, Phys. Rev. C 50 (1994) 2490.
[27] A. Gilbert, A.G.W. Cameron, Can. J. Phys. 43 (1965) 1446.
[28] W. Dilg, W. Schantl, H. Vonach, M. Uhl, Nucl. Phys. A 217 (1973) 269.
[29] A.V. Ignatyuk, K.K. Istekov, G.N. Smirenkin, Sov. J. Nucl. Phys. 29 (4) (1979) 450.
[30] A.V. Ignatyuk, J.L. Weil, S. Raman, S. Kahane, Phys. Rev. C 47 (1993) 1504.
[31] A.J. Koning, M.C. Duijvestijn, Nucl. Phys. A 744 (2004) 15.
[32] IAEA-EXFOR Experimental nuclear reaction data base, http://www.nds.iaea.org/exfor.